Meteorol Atmos Phys (2006)
DOI 10.1007/s00703-005-0170-7

Meteorology and Atmospheric Physics
Printed in Austria

[1] Center for Analysis and Prediction of Storms, University of Oklahoma, Norman, OK, USA
[2] School of Meteorology, University of Oklahoma, Norman, OK, USA
[3] Meteorological Research Institute, Seoul, Korea
[4] National Severe Storm Laboratory, Norman, OK, USA

A three-dimensional variational single-Doppler velocity retrieval method with simple conservation equation constraint

J. Gao[1], **M. Xue**[1,2], **S.-Y. Lee**[3], **A. Shapiro**[1,2], **Q. Xu**[4], and **K. K. Droegemeier**[1,2]

With 10 Figures

Received December 30, 2004; accepted November 23, 2005
Published online: July 31, 2006

Summary

In this paper, a new three-dimensional variational analysis scheme capable of retrieving three-dimensional winds from single Doppler observations of convective storms is developed. The method incorporates, in a single cost function, Doppler radar observations, a background field, smoothness and mass continuity constraints, and the residual of reflectivity or radial velocity conservation. By minimizing this cost function, an analysis with the desired fit to these constraints is obtained in a single procedure. In tests with both simulated and real thunderstorm cases, detailed structures of the storms are well retrieved in comparison with reference analysis.

Unlike most kinematic retrieval methods, our scheme is capable of directly dealing with data voids. When an analysis background is available, say from a proximity sounding, a wind profiler, or a numerical model forecast, the method naturally blends Doppler radar observations with it. Thus, a smooth transition is obtained between data-rich and data-void areas. These features, among others, are important if the analysis is to be used to initialize storm-scale numerical models or for diagnostic studies of storm structures.

1. Introduction

Doppler radar has long been a valuable observational tool in meteorology. It has the capability of observing, at high spatial and temporal resolution, the internal structure of storm systems from remote locations. However, direct measurements are limited to reflectivity, the radial component of velocity, and the spectrum width; there is no direct measurement of the complete three-dimensional (3-D) wind field. In order to gain a more complete understanding of storm dynamics, as well as to initialize storm-resolving numerical models, such information is necessary.

Many techniques for retrieving the unobserved wind components from single-Doppler radial velocity and perhaps also reflectivity data have been developed since the last decade (e.g., Tuttle and Foote, 1990; Sun et al, 1991; Liou et al, 1991; Qiu and Xu, 1992; Sun and Crook, 1997, 1998; Shapiro et al, 1995; Laroche et al, 1994; Weygandt et al, 1995, 2002; Zhang and Gal-Chen, 1996; Gao et al, 2001, Crook and Sun, 2004). A detailed review of these and other methods can be found in Shapiro et al (2003).

Qiu and Xu (1992) developed a simple adjoint method (SA) to retrieve 2-D wind field from the lowest-elevation scans, and tested using the Phoenix-II dataset and the Denver microburst dataset (Xu et al, 1994; 1995). As demonstrated in their studies, the use of data gathered over several radar scans reduces the under-determined

nature of the retrieval problem. Other non-Doppler radar information, such as surface wind and other observations, and equation constraints such as the mass continuity and smoothness constraints can be easily incorporated into the retrieval procedure. Because the SA method uses only the conservation equation(s) for reflectivity and/or radial velocity, the boundary conditions are readily available. The shortcoming is that it is difficult to deal with data voids in the initial tracer field which is needed to integrate the simple forward model equation.

The variational Doppler radar analysis system (VDRAS) for retrieval of three-dimensional wind, thermal, and hydrometeor fields was described and tested using simulated data of a warm rain convective storm and real dataset (Sun et al, 1991; Sun and Crook, 1997; 1998). This analysis system applies the 4-D variational data assimilation technique to a cloud-scale model. Radial velocity and reflectivity observations from one or more Doppler radars can be assimilated into the numerical model by minimizing the difference between the observations and the model predictions. A set of optimal initial conditions consisting of wind, thermal, and microphysical fields is determined as the model is optimally fitted to the observations. The application of this analysis system to different stages of the evolution of a simulated convective storm demonstrated that the detailed structure of wind, thermodynamics, and microphysics could be obtained with reasonable accuracy. However, the application of VDRAS to deep convective storms can present a great challenge because it is computationally too expensive to run in real time. Nevertheless, it was shown that the method could be applied to retrieve the low-level wind reasonable in real time successfully (Crook and Sun, 2004).

Qiu and Xu (1996) also applied a least-squares method by using the simple advection/conservation equation as a weak constraint. This more efficient method proved superior to the 2-D simple adjoint method. For the purpose of initializing numerical weather prediction (NWP) models, the vertical velocity is also required unless other fields are known perfectly (Weygandt et al, 1999; Nascimento and Droegemeier, 2002). Diagnostic studies using the retrieved data usually require information about vertical velocity as well. Typically, vertical velocity is obtained by integrating the mass continuity equation vertically from independently retrieved horizontal (or nearly horizontal) winds. However, the results often are poor (Gao et al, 1999a).

Gao et al (2001), and Xu et al (2001) extended the 2-D SA methods to a fully 3-D formulation, also using the 3-D anelastic mass continuity conservation equation as a weak constraint, so as to couple the three wind components. The method was tested using data from a simulated supercell storm and compared against the model ''truth''. It was shown that circulations inside and around the storms, including the strong updraft and associated downdraft, can be well retrieved. The SA method does require the integration of a simplified radial-component momentum equation and/or the reflectivity conservation equation forward, and their corresponding adjoint backward, many times in the minimization procedure. However, for a 3-D dense grid, the CPU time and memory requirements still can be significant.

In this work we seek to overcome this difficulty by using the reflectivity conservation equation, as a weak constraint in a 3-D setting. In the cost function, temporal and spatial derivatives are obtained using finite differences from two or three time levels of radar observations, and the equations are not integrated in time. Also, different from Qiu and Xu (1996), we include the background field as additional information, and use the more physical mass continuity equation constraints instead of the zero-divergence and zero-vorticity (weak) constraints. To test the performance of our method, we present single-Doppler wind retrievals using a simulated deep convective storm as well as radar observations of a real storm. For the simulated data case, the sensitivities of the retrieval to radar location and observation errors are examined and the analysis errors quantified against model ''truth''.

This paper is organized as follows: in Sect. 2, the new 3-D variational method is introduced. In Sect. 3, the method is tested with a set of idealized data sampled from a simulated supercell storm, and quantitative analysis errors are calculated against the model ''truth''. In Sect. 4, retrieval results from the May 17, 1981 Arcadia, Oklahoma supercell storm are presented. Finally, summary and concluding remarks are given in Sect. 5.

2. Description of retrieval method

Our method is based on a variational procedure in which we define a cost function, J, as the sum of the squared errors due to the misfit between observations and analyses, subject to certain constraints. Each constraint is weighted by a factor that accounts for its presumed accuracy. The cost function is minimized to yield an analysis that gives the best fit to the radar observation subject to background and other constraints. When a different form of the cost function is used, the analysis is usually different. The definition of the cost function and its subsequent minimization are key issues in variational analysis. The variational method makes use of the derivative of J with respect to the analysis variables, and thus J must be differentiable.

Designed for the analysis of 3-D wind fields from Doppler radar and other observations, our variational method described herein retrieves the 3-D time-mean (over the retrieval period) wind vector (u_m, v_m, w_m) from single-Doppler radar radial velocity (V_r^{ob}) and/or reflectivity (η^{ob}). The retrieval period is typically the interval comprising two or three radar volume scans over which the time tendency of radial velocity or reflectivity is evaluated (typically between 1 to 10 minutes depending on the radar scan strategy used).

The cost-function that we use is defined as follows:

$$J = J_E + J_{V_r} + J_B + J_D + J_S, \tag{1}$$

where the first term,

$$J_E = \frac{1}{2} \sum_{n=1 \text{ or } 2}^{N-1} W_E (E_n)^2 \tag{2}$$

measures the extent to which the three-dimensional reflectivity or radial velocity advection-diffusion (or conservation) equation,

$$\frac{\partial \eta}{\partial t} + u_m \frac{\partial \eta}{\partial x} + v_m \frac{\partial \eta}{\partial y} + w_m \frac{\partial \eta}{\partial z} - k_H \nabla_H^2 \eta - k_V \nabla_V^2 \eta - F_m = 0, \tag{3}$$

is satisfied. W_E in Eq. (2) is the weight for this term, more discussion on the choice of weights for the terms in Eq. (1) will be given later. The index n in Eq. (2) denotes the time level of the observation, and N is the total number of radar volume scans used in the retrieval.

The studies of Xu et al (1994), and Xu and Qiu (1995) examined the use of one or both of the radial velocity and reflectivity equations, in the form of Eq. (3), in the context of the 2-D SA method. When both are used, slightly better retrieval results were obtained (Xu and Qiu, 1995). When η is the radial velocity, then Eq. (3) represents a momentum equation with the term F_m representing other forcing terms not explicitly given in the equation. When η is the reflectivity, F_m then contains source and sink terms related to microphysical processes. Our procedure is formulated in a general way so that Eq. (3) can be applied to either radial velocity or reflectivity, or both.

In Eq. (2), u_m, v_m, and w_m are the time-mean (over the retrieval period) x, y, and z velocity components, which are the outcome of retrieval. In the terminology of optimal control theory, they are the control variables, and represent the time mean because the radar observations span over the retrieval period. It is assumed that this mean velocity causes, via advection, a significant part of the change in the "tracer" field, η. Here the "tracer" does not have to conserve because the "conservation" equation does include the effect of other non-conservative forcing or source/sink terms, denoted by F_m, which is to be retrieved as well.

Equation (3) includes horizontal and vertical diffusion terms, with eddy coefficients of k_H and k_V, which are assumed to be unknown constants to be retrieved. The term F_m, mentioned earlier, is a time-mean source term, also to be retrieved, and includes effects such as centrifugal and pressure gradient forces if the tracer is radial velocity, or sources and sinks of hydrometeors in association with microphysical processes, and the effects of terminal velocity (if this effect is not accounted for in the vertical advection process), if the tracer is reflectivity. In order to evaluate the terms in Eq. (3) using finite differences, bilinear-interpolation is performed to interpolate the observed reflectivity and/or radial velocity from the observation points (in radar spherical coordinates) to the analysis (Cartesian coordinate)

grid. The residual of Eq. (3), E_n, is computed according to

$$E_n \equiv \frac{1}{2\Delta t}\left(\eta_{\text{ob}}^{n+1} - \eta_{\text{ob}}^{n-1}\right) + \left(u_m \frac{\partial}{\partial x} + v_m \frac{\partial}{\partial y} + w_m \frac{\partial}{\partial z}\right)\eta_{\text{ob}}^{n} - \left(k_H \nabla_H^2 + k_v \nabla_v^2\right)\eta_{\text{ob}}^{n} - F_m, \quad (4)$$

where η_{ob}^{n} denotes the observed reflectivity or radial velocity at the n-th time level and Δt is the time interval between successive radar scans. All spatial derivatives are computed using the standard second-order centered difference scheme.

The second term, J_{V_r}, in Eq. (3) defines the distance between the analyzed temporal mean radial velocity, V_r, and the observed counterpart, $V_{r\,\text{ob}}$:

$$J_{V_r} = \frac{1}{2}\sum_n W_r (V_r - V_{r\,\text{ob}}^{n})^2. \quad (5)$$

W_r is the weight, and V_r is given by the forward operator $V_r = PQ(u_m, v_m, w_m)$, where Q is a linear interpolation operator that maps the 3-D Cartesian velocity (u_m, v_m, w_m) from the grid to observation points. At observation points, the winds are denoted by (u'_m, v'_m, w'_m). P is an operator that projects the winds (u'_m, v'_m, w'_m) to the radial direction and has the following form:

$$P(u'_m, v'_m, w'_m) = (xu'_m + yv'_m + zv'_m)/r, \quad (6)$$

where r is radial distance from the radar to the observation point. In doing so, all observed velocities, including their orientation, are used without any directional bias when η is the radial velocity. In another words, interpolation that may produce inaccurate averaged vectors is avoided. This issue does not exist for scalar reflectivity.

The other terms in the cost function have the following definitions:

$$J_B = \frac{1}{2}\left[\sum_{ijk} W_{ub}(u_m - u_b)^2 + \sum_{ijk} W_{vb}(v_m - v_b)^2 + \sum_{ijk} W_{wb}(w_m - w_b)^2\right], \quad (7)$$

$$J_D = \frac{1}{2}\sum_{ijk} W_D D^2, \quad (8)$$

$$J_S = \frac{1}{2}\left[\sum_{ijk} W_{us}(\nabla^2 u_m)^2 + \sum_{ijk} W_{vs}(\nabla^2 v_m)^2 + \sum_{ijk} W_{ws}(\nabla^2 w_m)^2\right]. \quad (9)$$

Here, J_B measures the fit of the variational analysis to the analysis background, and J_D imposes a weak anelastic mass continuity constraint on the analyzed wind field, where

$$D \equiv \frac{\partial \bar{\rho} u_m}{\partial x} + \frac{\partial \bar{\rho} v_m}{\partial y} + \frac{\partial \bar{\rho} w_m}{\partial z}, \quad (10)$$

and where $\bar{\rho}(z)$ is the mean air density chosen to be a function only of height. $D = 0$ is the anelastic mass continuity equation.

The last term in the cost function, J_s, is a spatial smoothness constraint that acts to both reduce the noise in the analyzed field as well as help to alleviate the under-determined nature of the problem. The effect of this smoothing term is similar to filters, either, as discussed in, e.g., Huang (2001), or implicit (e.g., Hayden and Purser, 1995) in the standard formulation of 3DVAR analysis. In the latter case, the filter is generally designed to model the effect of background error covariances so that the background can be effectively updated using the limited amounted of observations available. This produces yet relatively smooth analysis. Again, each of the terms in Eqs. (8)–(10) contains a weight, W.

The weights, W, which are assumed to be constant coefficients, are simplified forms of the inverse error covariances for each term. In general, these coefficients should be matrices proportional to the inverse of the error covariance matrices of the associated terms in the cost function. In storm-scale data assimilation, and especially for radar data, these error covariances are usually difficult to obtain. The accurate estimation of error statistics is one of the major challenges of variational data assimilation, especially for small scales where weather phenomena are often spatially and temporally intermittent.

By using constant weights, the spatial correlations are not included in the background error covariance matrices, though the effects

of spatial correlations of the same variable, as well as cross-correlations among variables, are achieved partially through the use of equation (conservation and mass continuity) and smoothness constraints. It is these constraints that make the retrieval of unobserved variables possible.

The actual choice of the values of weights should reflect the error statistics of each term. For all terms to be effective in the cost function, the weights should result in constraint terms that are of same or similar order of magnitude, as least when the optimization is close to convergence. For our purposes, the weight coefficients are chosen based on both the estimated standard deviation of observed radial wind and the perceived relative important of each term via trial and error numerical experimentation. Experience with the test cases presented herein suggests that the solutions obtained are not very sensitive to the precise values of W, and W can be treated as a tuning parameter (Hoffman, 1984). In one case, we will show that the analyses change by only a small amount when a particular W is halved or doubled.

To solve the above variational problem by direct minimization, we derive the gradient of the cost function with respect to the control variables (u_m, v_m, w_m, F_m, k_H, k_v). Taking the variation of J with respect to u_m, v_m, w_m, F_m, k_H, and k_V at each grid point, we obtain the components of the gradient of as follows:

$$\left(\frac{\partial J}{\partial u_m}\right)_{ijk} = \sum_n (W_E E)_n \frac{\partial \eta^n_{\rm ob}}{\partial x} + W_r \frac{x}{r}\frac{\partial Q}{\partial x}(V^n_r - V^n_{r\,\rm ob}) + W_{ub}(u_m - u_b) - W_D \bar{\rho}\frac{\partial D}{\partial x} + W_{su}\nabla^2(\nabla^2 u_m), \quad (11a)$$

$$\left(\frac{\partial J}{\partial v_m}\right)_{ijk} = \sum_n (W_E E)_n \frac{\partial \eta^n_{\rm ob}}{\partial y} + W_r \frac{y}{r}\frac{\partial Q}{\partial y}(V^n_r - V^n_{r\,\rm ob}) + W_{vb}(v_m - v_b) - W_D \bar{\rho}\frac{\partial D}{\partial y} + W_{sv}\nabla^2(\nabla^2 v_m), \quad (11b)$$

$$\left(\frac{\partial J}{\partial w_m}\right)_{ijk} = \sum_n (W_E E)_n \frac{\partial \eta^n_{\rm ob}}{\partial z} + W_r \frac{z}{r}\frac{\partial Q}{\partial z}(V^n_r - V^n_{r\,\rm ob}) + W_{wb}(w_m - w_b) - W_D \bar{\rho}\frac{\partial D}{\partial z} + W_{sw}\nabla^2(\nabla^2 w_m), \quad (11c)$$

$$\left(\frac{\partial J}{\partial F_m}\right)_{ijk} = -\sum_n (W_E E)_n, \quad (11d)$$

$$\left(\frac{\partial J}{\partial k_H}\right)_{ijk} = \sum_n (W_E E)_n \nabla^2_H \eta, \quad (11e)$$

$$\left(\frac{\partial J}{\partial k_v}\right)_{ijk} = \sum_n (W_E\, E)_n \frac{\partial^2 \eta}{\partial z^2}. \quad (11f)$$

In the above derivation, the commutation formula

$$\sum \alpha \nabla \beta = -\sum \beta \nabla \alpha \quad (12)$$

of the finite-difference analog is used (Sasaki, 1970).

After the gradients of the cost function are obtained, the data retrieval problem can be solved via the following steps:

(1) Choose a first guess for the control vector $Z = (u_m, v_m, w_m, F_m, k_H, k_V)$ and calculate the cost function, J, using Eqs. (1), (2), (5), (7), (8) and (9);

(2) Calculate the gradients $\left(\frac{\partial J}{\partial u_m}, \frac{\partial J}{\partial v_m}, \frac{\partial J}{\partial w_m}, \frac{\partial J}{\partial F_m}, \frac{\partial J}{\partial k_H}, \frac{\partial J}{\partial k_V}\right)$ according to Eq. (11a) through (11f);

(3) Use the quasi–Newton minimization algorithm (Navon, 1987) to obtain updated values of the control variables,

$$Z^l_{ijk} = Z^{l-1}_{ijk} + \alpha \cdot f\left(\frac{\partial J}{\partial Z}\right)_{ijk}, \quad (13)$$

where l is the number of iterations, α is the optimal step size obtained by the so-called ''line-search'' process in optimal control theory (Gill et al, 1981), and $f(\partial J/\partial Z)_{ijk}$ is the optimal descent direction obtained by combining the gradients from several former iterations;

(4) Check whether the optimal solution has been found by computing the norm of the gradients and the value of J to see if they are less than prescribed tolerances. If the criteria

are satisfied, stop the iteration and output the optimal control vector (u_m, v_m, w_m, F_m, k_H, k_v);

(5) If the convergence criteria are not satisfied, steps 1 through 4 are repeated using updated values of (u_m, v_m, w_m, F_m, k_H, k_V) as the new guess. The iteration process is continued until a suitably converged solution is found.

For radar scans at nonzero elevation angles, the fall speed contributes to the Doppler estimate of radial velocity. The observations of radial velocity are adjusted to remove this contribution using

$$v_{r\,\mathrm{ob}} = v^a_{r\,\mathrm{ob}} + w_t \sin\theta, \tag{14}$$

where $v^a_{r\,\mathrm{ob}}$ is the radial velocity actually observed by the radar, $v_{r\,\mathrm{ob}}$ is the true radial velocity of the air, w_t is the terminal velocity of precipitation, and θ is the elevation angle (0° is horizontal). An empirical relationship is used to relate the reflectivity, R, and raindrop terminal fall velocity (Foote and duToit, 1969; Atlas et al, 1973):

$$w_t = 2.65\left(\frac{\rho_0}{\rho}\right)R^{0.114}, \tag{15}$$

where ρ is the air density and ρ_0 is its surface value. Note that, in this formulation, w_t is positive downwards.

3. Experiment design and statistics

3.1 Experiment design

To evaluate the performance of our variational single Doppler velocity retrieval technique, we utilize a set of numerical model simulated single-Doppler radar data. The Advanced Regional Prediction System (ARPS, Xue et al, 1995; Xue et al, 2000) is used here to perform a two-hour simulation using a sounding near Del City, Oklahoma on 20 May 1977. The simulation starts from a thermal bubble placed in a horizontally homogeneous base state specified from the sounding. The model grid comprises $67 \times 67 \times 35$ grid points with a uniform grid interval of 1 km in the horizontal and 0.5 km in the vertical (detail of model settings can be found in Gao et al, 2001). Figure 1 shows horizontal and vertical cross-sections of storm-relative wind, vertical velocity, and reflectivity at two hours. A strong rotating updraft (with maximum

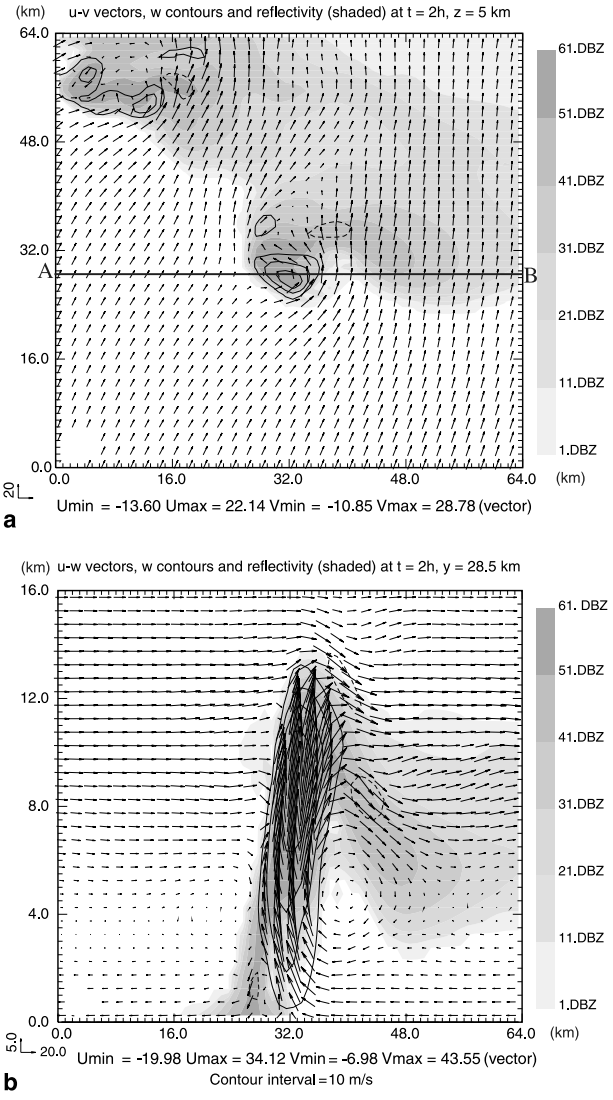

Fig. 1. The ARPS model simulated wind vectors, vertical velocity w (contours) and simulated reflectivity (shaded) fields of the 20 May 1977 supercell storm at 2 hours. (**a**) Horizontal cross-section at z = 5 km; (**b**) Vertical cross-section at y = 28.5 km, i.e., through line A–B in (a)

vertical velocity exceeding 34 m/s) and associated low-level downdraft are evident near the center of the domain, while the left mover is about to exit the domain. The evolution of the simulated storm is qualitatively similar to that described by Klemp and Wilhelmson (1981), and by two hours, the storm has attained a structure typical of mature supercells.

The simulated 3-D convective-scale wind and reflectivity fields at two hours are sampled by a single pseudo-Doppler radar located at several different locations at ground level. Using a bilinear interpolation scheme, the wind compo-

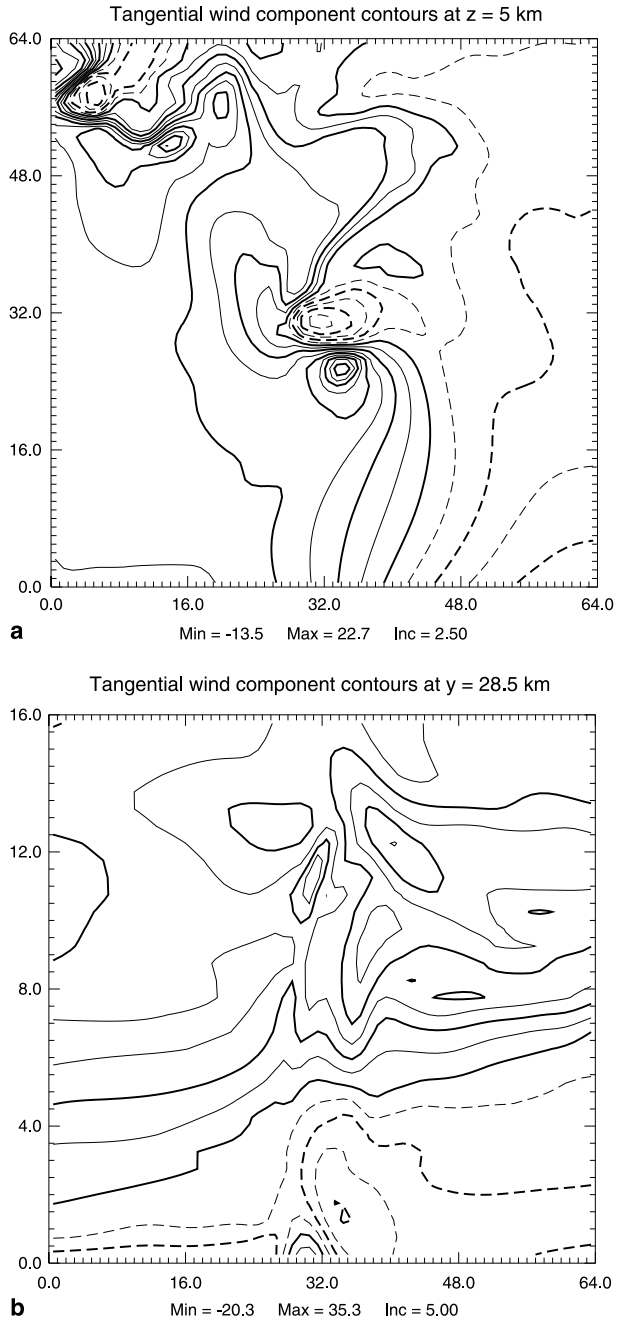

Fig. 2. The contours of the ARPS model simulated tangential wind component v_ϕ. (**a**) Horizontal cross-section at z = 5 km; (**b**) vertical cross-section at y = 28.5 km

nents are first interpolated from the model grid points to the radar sampling locations. Then they are synthesized to obtain radial velocities according to Eq. (6). The reflectivity field (used as tracer) also is interpolated to the sampling locations along the radar beams using the same procedure. The elapsed times for the volume scans of the pseudo-radar are neglected, and thus we assume that the radial wind observations are instantaneous. The simulated radial velocity data at time level 7200 s are used as observations, and simulated reflectivity data at 6900 s 7200 s and 7500 s are used as the tracer in Eq. (3). The time interval between reflectivity scans is similar to that of NEXRAD.

When radar data are used to initialize a numerical weather prediction model, a complete description of the wind and other meteorological variables is needed in the entire model domain. Even for diagnostic studies, consistent analyses outside the area containing radar data areas also are desirable. Here the sounding profile used to define the storm-environment for the numerical simulation is incorporated into the cost function as the analysis background.

The parameter settings used for the retrievals are $W_{rm} = 1$, $W_{ub} = W_{vb} = 5\times10^{-2}$, $W_{wb} = 0.0$, $W_D = 1/(0.5\times10^{-3})^2$, and $W_{us} = W_{vs} = W_{ws} = 10^{-2}$. These values are chosen so that the constraints have proper orders of magnitude after being multiplied by the corresponding coefficients. These parameters also indicate the relative importance of each term in the cost function.

3.2 Statistical measures of analysis errors

To measure the accuracy of single-Doppler radar retrievals, we calculate the RMS error and relative RMS error between the retrieved 3-D velocity and the model-generated "truth". However, the complete 3-D wind components (u, v, w) consist of both the observed radial wind (v_r) and unobserved tangential and polar winds. Because the quality of the retrieval is based largely on the quality of the unobserved wind components, we project the retrieved horizontal winds back to the tangential direction to obtain the azimuthal velocity component, v_ϕ (Weygandt et al, 2002). We calculate the RMS and relative RMS errors of v_ϕ according to

$$\mathrm{RMS} = \left[\frac{1}{N}\sum_{i=1}^{N}\left(v_\phi - v_\phi^{\mathrm{ref}}\right)_i^2\right]^{1/2}, \tag{16}$$

$$\mathrm{RRE} = \left[\sum_{i=1}^{N}\left(v_\phi - v_\phi^{\mathrm{ref}}\right)_i^2 \Big/ \sum_{i=1}^{N}\left(v_\phi^{\mathrm{ref}}\right)_i^2\right]^{1/2}. \tag{17}$$

Here the summation is over the total number of grid points, N, and the superscript ref stands for the reference or true field sampled from the ARPS model simulation. Because Doppler radars usually operate at low elevation angles, vertical velocities are mostly unobserved. We therefore also calculate the RMS and relative RMS errors of the vertical velocities, which are mostly retrieved. In addition, the Spearman's rank correlation coefficients (CC) of azimuthal and vertical winds (between the retrieved and reference fields) also are calculated by the following formula, which is given for the azimuthal velocity as an example:

$$\rho(v_\phi, v_\phi^{\mathrm{ref}}) = \left[\sum_{i=1}^{N}(v_\phi - \overline{v_\phi})\left(v_\phi^{\mathrm{ref}} - \overline{v_\phi^{\mathrm{ref}}}\right)\right] \times \left[\sum_{i=1}^{N}(v_\phi - \overline{v_\phi})^2 \sum_{i=1}^{N}\left(v_\phi^{\mathrm{ref}} - \overline{v_\phi^{\mathrm{ref}}}\right)^2\right]^{-1/2}. \quad (18)$$

4. Experiments with model-simulated observations

In this section, we present the results from the set of experiments outlined in the previous section. The analysis domain is the same as the ARPS integration domain described earlier.

To obtain well-converged solutions, 350 iterations are used in all experiments.

4.1 Control experiment

We examine first the control experiment (CNTL), for which all constraints discussed in Sect. 2 are included. The first guesses for all the wind components and the forcing term of the simplified equation are set to zero, and the first guesses for the horizontal and vertical diffusion coefficients are set to $400\,\mathrm{ms}^{-2}$. The retrieval results are presented in Figs. 3 and 4. Comparing Fig. 3 with the true fields in Fig. 1, we see that all important features in the horizontal wind fields are retrieved, including flow curvature around the main rotating updraft as well as convergence on the upstream side of the updraft (Fig. 3a). In the vertical cross-section, the general

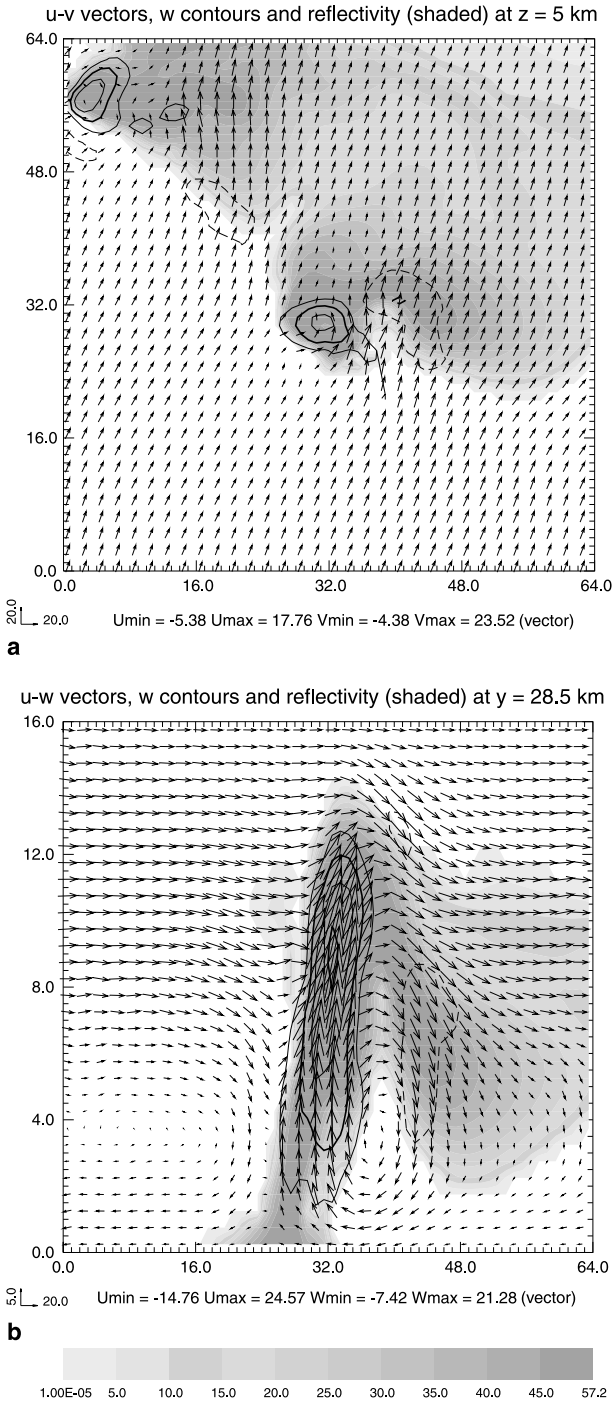

Fig. 3. The wind vectors, the contours of difference vertical velocity between the retrieved wind and the referenced one. Others are same as Fig. 1. The first guess wind is zero

structure of the updraft is well retrieved at all levels, though the low-level downdraft immediately below the updraft is less obvious. The retrieved fields show a deeper downdraft circulation that descends from about 6 km and is located further west of the main updraft. The vertical

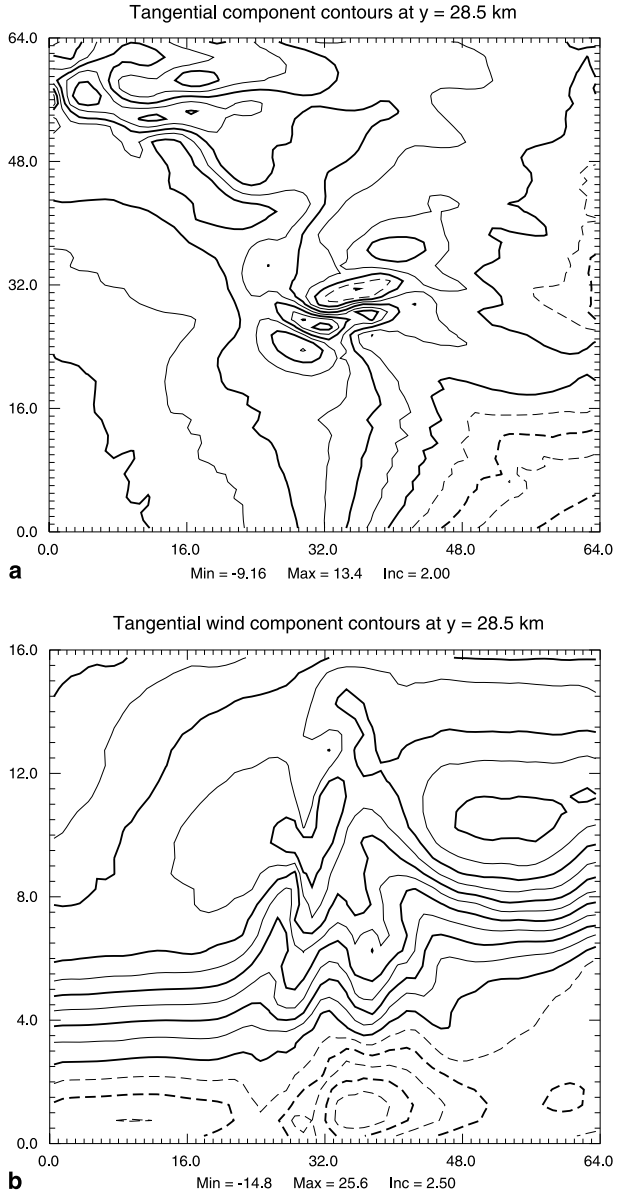

Fig. 4. The contours of retrieved component v_ϕ in CNTL. As Fig. 2

circulation on the downstream side (with respect to the upper-level flow), with strong descending flow below 10 km in the retrieval (Fig. 3b), agrees quite well with the reference field (Fig. 1b). The mean relative RMS error is small for the cross-beam wind (0.378 m/s, see Table 1), and the correlation between the retrieval and the truth peaks at 0.914. The RMS error for the vertical velocity is larger (0.762 m/s) and the correlation coefficient is only 0.691. Still, the general vertical flow structure is quite reasonable (Fig. 3). This is so because most of the errors are in the amplitude while the phase error is relatively small. The maximum retrieved vertical motion is weaker than the true one.

Table 1. List of experiments with different radars

Experiments	Cross-beam wind (v_ϕ)			Vertical wind (w)		
	RMS	RRE	CC	RMS	RRE	CC
CNTL	5.352	0.378	0.914	2.915	0.762	0.691
Radar 2	5.549	0.393	0.916	3.020	0.790	0.664
Radar 3	5.658	0.423	0.912	3.083	0.807	0.632
Radar 4	5.772	0.474	0.896	3.225	0.844	0.596
Radar 5	5.657	0.521	0.875	3.348	0.876	0.579
Radar 6	5.358	0.539	0.813	3.194	0.836	0.596
Radar 7	5.393	0.496	0.766	3.095	0.810	0.624
Radar 8	4.891	0.448	0.884	3.253	0.851	0.544

To clearly show how much of the unobserved wind field is retrieved, the tangential wind component v_ϕ is plotted in Fig. 4. The main positive–negative couplet near the domain center agrees well with the true one in Fig. 2, while the tangential wind component of left-moving storm, the storm cell near the northwest corner of the analysis domain, is less well retrieved. The proximity to the lateral boundary, the more rapid cell movement, and the relatively greater distance from the radar are believed to be the contributing factors.

To further examine in detail the quality of this retrieval, the changes of the cost function and its

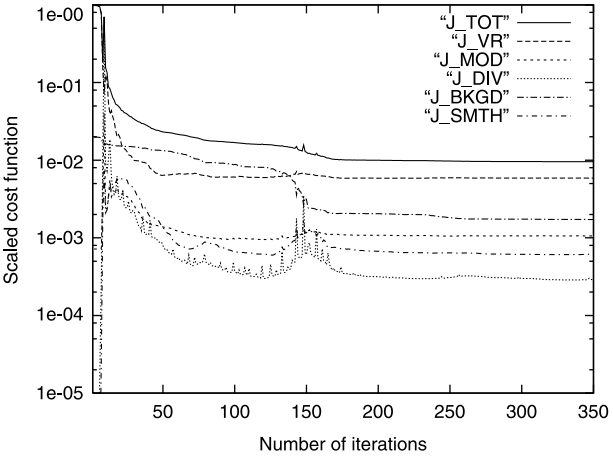

Fig. 5. The scaled total cost function (J_k/J_0) and contribution of each constraint as a function of the number of iterations. The first guess wind is zero. J_TOT stands for the total cost function, J_VR, J_MOD, J_DIV and J_BKGD stands for contribution from the mean radial velocity, the simple conservation equation, the mass continuity, and background constraints, respectively

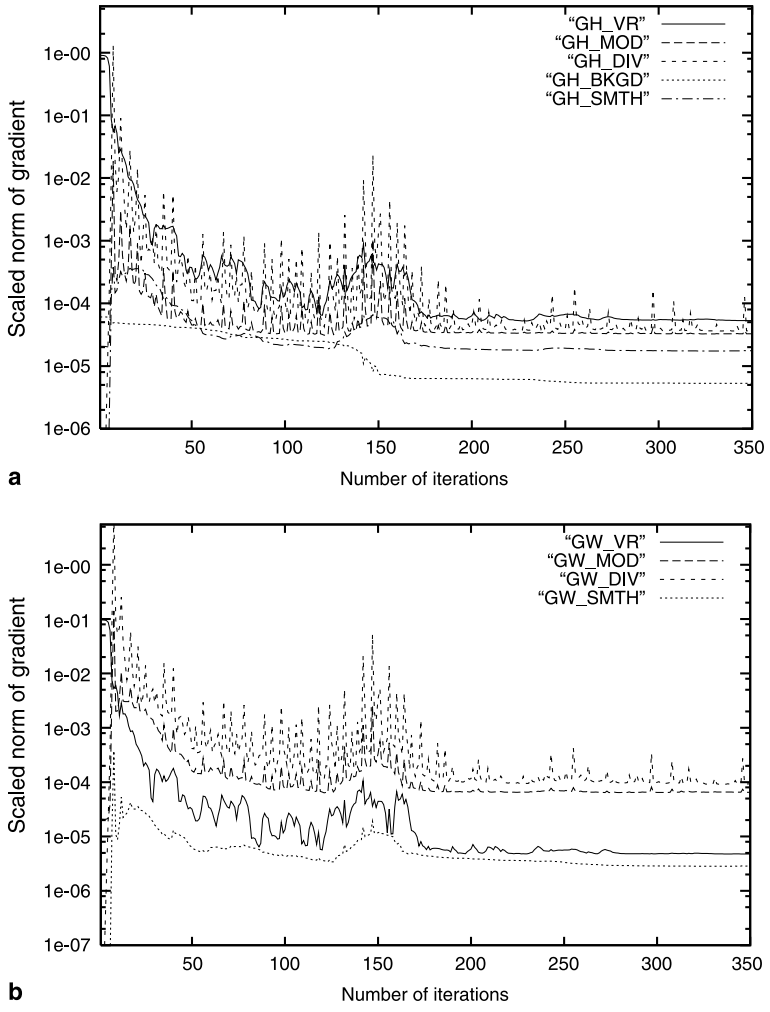

Fig. 6. The scaled norm of gradient of each constraint as a function of the number of iterations. (**a**) The contribution to horizontal wind, (**b**) the contribution to vertical velocity. The first guess wind is zero. GH_VR, GH_MOD, GH_DIV and GH_BKGD stand for contribution from the mean radial velocity, the simple conservation equation, the mass continuity, and background constraints to the retrieval of horizontal wind respectively. GW_VR, GW_MOD, and GW_DIV stand for contribution from the mean radial velocity, the simple conservation equation, and the mass continuity constraints to the retrieval of vertical velocity, respectively

gradient norm for each constraint, as a function of iteration number, are presented in Figs. 5 and 6. It can be seen that the cost function for the background constraint changed by only one order of magnitude, while the cost functions for the other constraints, including the simple conservation equation, mean radial velocity, and mass continuity constraints, are reduced by more than four orders of magnitude during the minimization. This indicates that the background constraint contributes less to the retrieval than any of the other constraints.

Figure 6a shows that the norm of the gradient of the background constraint is smallest among all constraints for nearly all iterations. Note that the background constraint does not have any contribution to the retrieval of vertical velocity because the background w is zero and is not used as a constraint. Comparing Fig. 6a with 6b, the contribution of the radial velocity constraint to the horizontal wind retrieval is of the same order of magnitude as the other constraints, except the background. The contribution of the radial velocity constraint to the vertical velocity retrieval, however, is significantly less than that of the other constraints. This is because Doppler radars usually operate at relatively low elevation angles, with the horizontal winds being much better observed than the vertical winds. Hence, the cost function corresponding to the radial velocity constraint is more sensitive to horizontal winds than to vertical winds, and therefore the horizontal wind component is easier to retrieve with the help of this constraint. Thus the retrieved w tends to be less accurate. Comparing Fig. 6a with 6b, the conservation equation and mass continuity constraints play about the same role for the retrieval of either the horizontal or vertical wind. More precisely, apart from the background term, the radial velocity constraint is most important

(the contribution to the gradient of the cost function is the largest) for the horizontal wind retrieval, while the mass continuity constraint is the most important to the retrieval of vertical velocity.

4.2 Sensitivity to radar position

Lazarus et al (1999), and Liou et al (2001) report that the quality of the single Doppler velocity retrieval depends on the radar location in their cases. Their conclusions were based on the retrieval of idealized divergent flows. For supercell-type convection, where the flow is often dominated by the rotational wind component, the conclusion may be different. In this section, we examine the sensitivity of wind retrieval to the radar location using the simulated storm from the previous section.

Similar to Liou et al (2001), a total of 9 virtual radars are placed in different locations relative to the primary storm cell. Our variational scheme is applied to data from each of these radars. Figure 7 illustrates the relative positions of these radars with respect to the retrieval domain. The main storm cell is near the center of domain at the data collection time. For the particular flow pattern shown in Fig. 1a, each radar observes a different portion of the 3-D wind vector. The test results for these 9 radars are listed also in Table 1, which shows that the mean relative RMS error of the retrieved tangential wind does not change much with radar location, and that the correlation coefficient between the retrieval and truth remains relatively high in all cases, with a minimum value of 0.766. This indicates that the retrieved cross-beam wind is not very sensitive to the radar positions for the current case. For vertical velocities, the relative RMS errors are larger, but the correlation coefficients between the retrieved and true vertical velocities change only by 0.15, with the minimum being 0.544. The vertical velocity therefore appears slightly more sensitive to the radar position as would be expected. In general, the retrieval for this deep convection case is less sensitive to radar location than reported by Lazarus et al (1999) and Liou et al (2001). This is probably because the horizontal flow in our current supercell case is mostly rotational and more isotropic than the flows examined in their studies. The conclusion may not be different if we focus on low-level flows where convergence along the gust front tends to be stronger, or in the case of quasi–symmetric tropical hurricane.

4.3 Sensitivity to weights and the role of individual constraints

As noted earlier, the weights of individual terms in the cost function are selected based on an

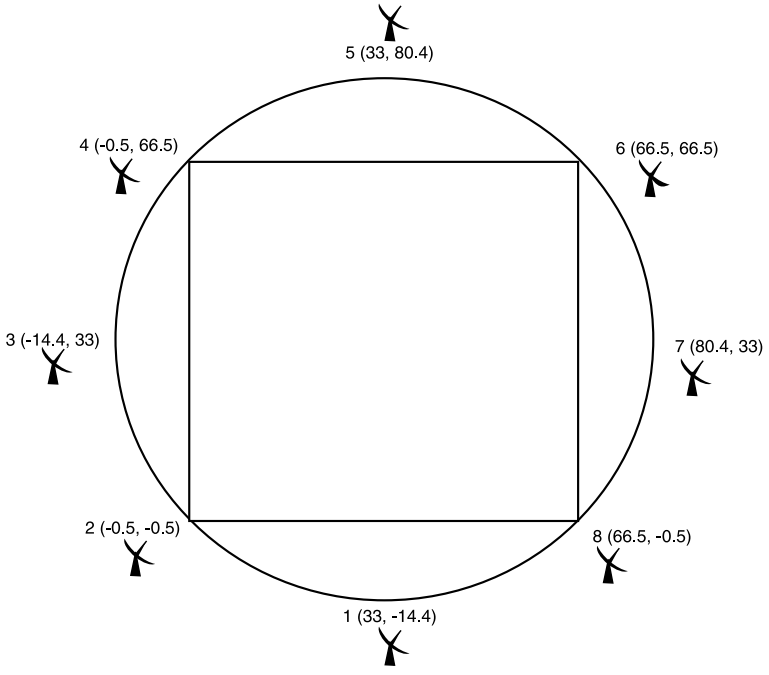

Fig. 7. Locations of the eight assumed radars that sample radial wind observation from the ARPS two hours run in Fig. 1. The square is the ARPS integration domain

estimate of the error characteristics of each term, and on numerical experimentations. A question is then raised regarding how important the choices of these weights are to the quality of the retrieval. This problem is examined in this section with regard to the sensitivities of the retrieval to the weights. For an extensive examination, we change these parameters individually in the range of 0.1 to 10 times the value of control run. The results are summarized in Table 2, which also includes the errors of the control run.

The variations in the statistics are within 15% of the control for most of the weights (except for W_D), even when each of them is increased or decreased by a factor of 10. In general, the retrievals are not very sensitive to the values of these weights, especially to the weights of mean radial wind constraint, smoothness and background constraints. When the weight of the smoothness constraint, W_S, is increased by a factor of 10, the statistics improve in term of RMS errors; when it is decreased by a factor of 10, the statistics of retrieval is significantly reduced. This finding agrees generally with those of Sun and Crook (1997; 1998) and Xu et al (1996; 2001).

As suggested in Gao et al (2001), the role of the anelastic mass continuity constraint is very important for the retrieval of vertical velocity. However, increasing the weight W_D by a factor of 10 makes the retrieval of the horizontal tangential wind much worse, even though the statistics for the vertical velocity are better; decreasing weight W_D 10 times slightly improves the retrieval of the tangential wind, but the retrieval for vertical velocity is worse. The retrieval is therefore most sensitive to the weight of the mass continuity constraint. Objectively, the order of magnitude of this weight should be close to the inverse of 10^{-4} to 10^{-3}, the magnitude of divergence associated with mesoscale, or stormscale flows. The choice of these weights significantly different from these values would make the retrieval worse.

Decreasing the weight of the simple reflectivity conservation equation reduces the quality of the retrieval according to the statistics in Table 2. The simple equation helps in retrieving detailed flow features of the storm, associated with, e.g., the low-level cold pool (picture not shown). The retrieval therefore seems to be also relatively sensitive to the weight of the conservation equation.

Table 2. List of experiments for different weight settings

Experiment	Action	Tangential wind (V_ϕ)			Vertical wind (w)		
		RMS	RRE	CC	RMS	RRE	CC
CNTL	×1	5.352	0.378	0.914	2.915	0.762	0.691
W_S	×10	5.317	0.375	0.919	2.888	0.756	0.686
	/10	5.462	0.386	0.911	3.079	0.806	0.663
W_R	×10	5.385	0.380	0.913	2.924	0.765	0.694
	/10	5.321	0.376	0.915	3.047	0.797	0.652
W_B	×10	5.900	0.416	0.911	3.287	0.860	0.547
	/10	6.053	0.427	0.902	3.000	0.785	0.676
W_D	×10	10.06	0.710	0.853	2.761	0.722	0.721
	/10	5.346	0.377	0.917	3.319	0.868	0.640
W_E	×10	7.992	0.564	0.847	3.524	0.922	0.588
	/10	5.458	0.358	0.922	2.339	0.612	0.804

Table 3. List of experiments with different observations errors

Experiments	Error of radial velocity	Tangential wind (V_ϕ)			Vertical wind (w)		
		RMS	RRE	CC	RMS	RRE	CC
CNTL	No error	5.352	0.378	0.914	2.915	0.762	0.691
ERR1	$\alpha = 0.3$	5.461	0.385	0.919	2.932	0.767	0.662
ERR2	$\alpha = 0.6$	5.584	0.394	0.908	3.349	0.876	0.515
ERR3	$\alpha = 1.0$	6.184	0.436	0.878	3.997	1.046	0.280

4.4 Sensitivity to data error

In reality, radial wind observations can contain large errors, both a bias type (e.g., ground clutter and anomalous propagation) and random errors. It is, however, very difficult to account for such errors in detail. Thus, we test in this section the quality of the retrieved fields when radar observations are subject to random observational errors. Similar to Gao et al (2001), we use $\widetilde{V_r} = (1 + \alpha\varepsilon)V_r$ as the observations, where ε represents random numbers between -1 and $+1$ and α is a specified positive number representing the relative magnitude of the error.

The error of retrieved field are given in Table 3, which shows that the retrieved vertical velocity is more sensitive to observational error than the tangential wind. Nevertheless, the general features of the 3-D wind field can be retrieved in all of these cases. It is worth mentioning that when α is increased to 1.0, i.e., when the relative errors are 100%, most of the key flow patterns in the truth are still recognizable, even though the correlation coefficient is rather small (Fig. 8). This shows that the method is rather robust even for such large random observation errors.

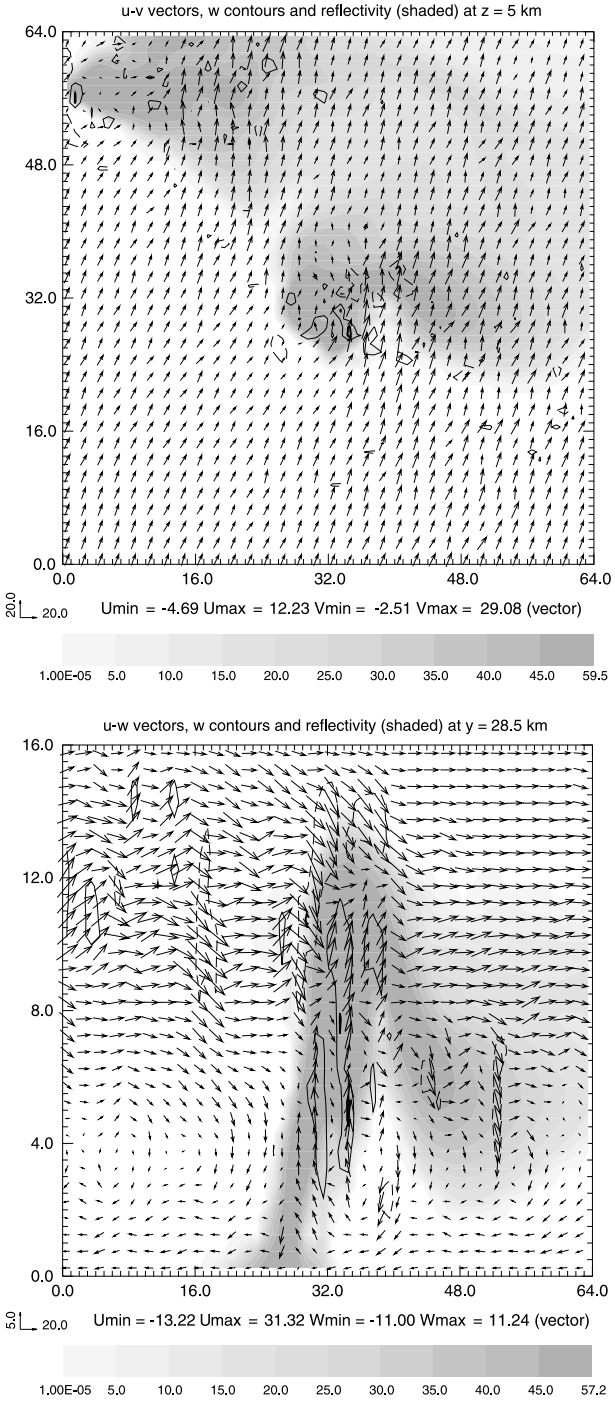

Fig. 8. The retrieved wind vectors and the contours of vertical velocity w when random errors are 100%. Others are same as Fig. 1. The first guess wind is zero

5. Test with to an observed storm case

In the previous section, we discussed results from a set of idealized experiments using model-generated pseudo observations. To demonstrate the effectiveness of the variational method for real data, we apply it to the 17 May 1981 Arcadia, Oklahoma (OK), supercell storm (Dowell and Bluestein, 1997). Twelve coordinated dual-Doppler scans were obtained from the Norman and Cimarron, OK S-band Doppler radars over a one-hour period spanning the pre-tornadic phase of the storm. Using the variational dual-Doppler analysis technique developed by the authors (Gao et al, 1999a), we performed a detailed dual-Doppler analysis of this storm. The analysis grid comprises $83 \times 83 \times 37$ grid points and the grid interval is 1 km in the horizontal and 0.5 km in the vertical. This dual-Doppler analysis will be used to verify the single-Doppler retrieval.

Figure 9 shows horizontal and vertical cross-sections in the dual-Doppler radar analysis of wind vectors, vertical velocity (vertical section is plotted through line A–B in Fig. 9a) and reflectivity at 1641 CST on May 17, 1981. A strong rotating updraft and the associated low-level downdraft are evident near the center of the vertical cross-section. A cold outflow originates from the rear flank downdraft that exhibits two maximum centers flanking the occlusion point of

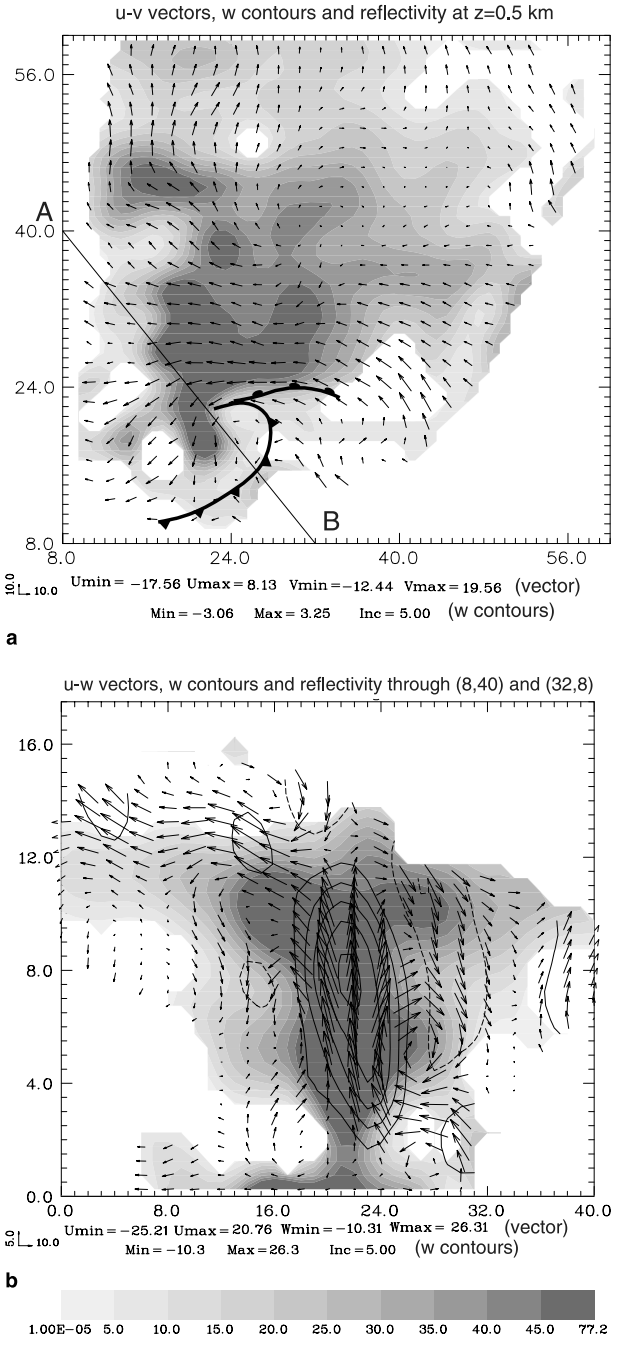

Fig. 9. Wind vectors, vertical velocity (contours) retrieved using the variational dual-Doppler analysis method for Arcadia, OK 17 May 1981 tornadic storm. (**a**) Horizontal cross-section at z = 0.5 km, (**b**) vertical cross-section through line A–B in panel (a). The shading area is reflectivity

the gust fronts. Ahead of this outflow is the rear flank gust front that is associated with surface convergence and a vertical velocity maximum. The reflectivity field shows a hook-echo pattern is consistent with the retrieved flow. Such a flow structure is typical of a tornadic supercell storm with strong low-level rotation (Lemon and Doswell, 1979).

For the single-Doppler velocity retrieval, the analysis domain is the same as that of dual-Doppler analysis. The background field is defined from a nearby sounding from Tuttle, Oklahoma. An initial guess of zero is used in this experiment, and the minimization is stopped after 350 iterations. Data at two time levels, specifically, at 1641 CST and 1645 CST from Cimarron, OK, are used by our single-Doppler velocity retrieval.

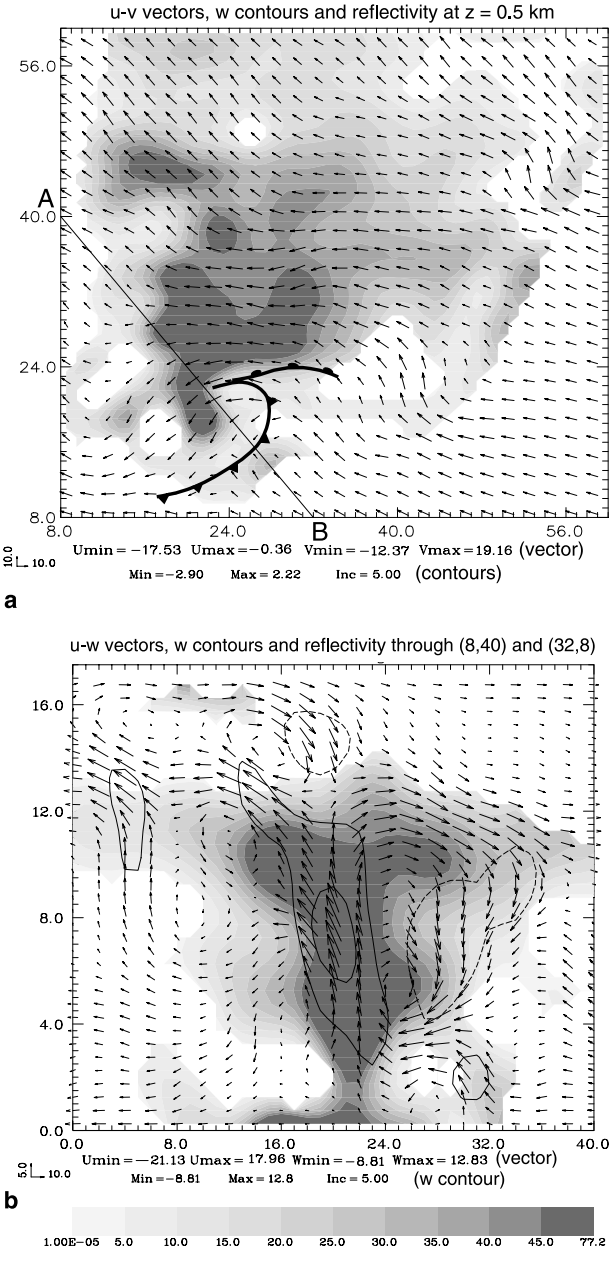

Fig. 10. As Fig. 9, but for single Doppler velocity retrieval using the radar data from Cimarron, OK

Figure 10 shows the retrieved fields (see caption for more details). Compared with Fig. 9, we can see that all significant features in the horizontal winds, i.e., the curvature around the rotating updraft and the convergence of wind fields, are well recovered. The main updraft is seen to originate ahead of the low-level gust front and in general matches the areas of maximum reflectivity. However, the retrieved maximum updraft is only about 12.83 m/s (Fig. 10b), or much lower than the dual-Doppler analysis value of about 26.31 ms^{-1} (Fig. 9b). The main downdraft is located below the updraft core and is collocated with a region of high reflectivity behind the gust front. These features suggest that both the horizontal and vertical flows are kinematically consistent and agree very well with the dual-Doppler analysis given in Fig. 9. A smooth transition exists between area where data is provided by the radar, and the area where only a background sounding is available.

6. Conclusions

In this paper, a new three-dimensional variational analysis scheme designed for retrieving three-dimensional winds from single-Doppler radar observations of convective storms is developed. The method incorporates observation (including radar radial velocity), background, smoothness, and mass continuity constraints as well as reflectivity and/or radial velocity conservation equation(s) in a single cost function. The cost function is minimized through a variational procedure to obtain an analysis with the desired fit to these constraints. This method is closely related to the three-dimensional simple-adjoint (SA) method developed earlier (Gao et al, 2001). Specifically, the same conservation equation is used in both method, but the SA method involves time integration of the conservation equation and its adjoint in the iterative minimization procedure. Even though the equations are relatively simple, such integrations for many times are still rather expensive in three dimensions. In cases where the regions of significant radar echoes are small and discontinuous, the portions of computational domain in which this conservation equation can be integrated over the retrieval period can become quite small, hence limiting the effectiveness of the conservations equation constraints. The current method forsakes the time integration of the conservation equation, but uses the equation as a weak constraint directly and evaluates the time tendency term in the equation with finite difference between two radar observation times. In doing so, the above two problems are alleviated.

The method is tested against a simulated data set as well as real radar observations of supercell storms. In both cases, detailed structures of the storms were well retrieved in comparison with the model truth and dual Doppler analysis.

Unlike most kinematic methods of wind retrieval, our method is capable of adequately dealing with data voids. When an analysis background is available, the method naturally blends the Doppler radar observations with the background. A smooth transition is obtained between data-rich and data-void areas in our experiment. These features are considered important for the analysis to be usable for initializing storm-scale numerical models as well as for diagnostic studies of storm structures. It is our plan to generalize our variational analysis procedure to include additional data sources, and to introduce additional dynamic constraints in the cost function so that thermodynamic fields can be retrieved simultaneously with the winds.

Acknowledgements

This research was supported by NSF grants ATM 03-31756, ATM 01-29892, ATM 99-81130, EEC 03-13747, and DOT-FAA grant NA17RJ1227-01. The first author is grateful for many helpful discussions with Dr. Jiandong Gong when he was a visiting scientist of Cooperative Institute of Mesoscale Meteorological Studies, University of Oklahoma.

References

Atlas D, Srivastava RC, Sekhon RS (1973) Doppler radar characteristics of precipitation at vertical incidence. Rev Geophys Space Phys 11: 1–35

Crook NA, Sun J (2004) Analysis and forecasting of the low-level wind during the Sydney 2000 forecast demonstration project. Wea Forecast 19: 151–167

Dowell DC, Bluestein HB (1997) The Arcadia, Oklahoma, storm of 17 May 1981: analysis of a supercell during tornadogenesis. Mon Wea Rev 125: 2562–2582

Foote GB, duToit PS (1969) Terminal velocity of raindrops aloft. J Appl Meteor 8: 249–253

Gao J, Xue M, Shapiro A, Droegemeier KK (1999a) A variational method for the analysis of three-dimensional wind fields from two Doppler radars. Mon Wea Rev 127: 2128–2142

Gao J, Xue M, Shapiro A, Xu Q, Droeegemeier KK (1999b) Simple adjoint retrievals using WSR-88D radar data. Preprints, 8th Conf. on Mesoscale Processes, Boulder, Colorado, Amer Meteor Soc pp 338–340

Gao J, Xue M, Shapiro A, Xu Q, Droegemeier KK (2001) Three-dimensional simple adjoint velocity retrievals from single Doppler radar. J Atmos Ocean Tech 18: 26–38

Gill PE, Murray W, Wright MH (1981) Practical optimization. New York: Academic Press, 401 pp

Hayden CM, Purser J (1995) Recursive filter objective analysis of meteorological fields: applications to NESDIS operational processing. J Appl Meteor 34: 3–15

Hoffman RN (1984) SASS wind ambiguity removal by direct minimization. Part II: Use of smoothness and dynamical constraints. Mon Wea Rev 112: 1829–1852

Huang X-Y (2001) Variational analysis using spatial filters. Mon Wea Rev 128: 2588–2600

Kessler E (1969) On the distribution and continuity of water substance in atmospheric circulation. Meteor Monogr 10(32), Amer Meteor Soc

Klemp JB, Wilhelmson RB, Ray PS (1981) Observed and numerically simulated structure of a mature supercell thunderstorm. J Atmos Sci 38: 1558–1580

Laroche S, Zawadzki I (1994) A variational analysis method for retrieval of three-dimensional wind field from single Doppler radar data. J Atmos Sci 51: 2664–2682

Lazarus S, Shapiro A, Droegemeier KK (1999) Analysis of the Gal-Chen-Zhang single-Doppler velocity retrieval. J Atmos Oceanic Technol 16: 5–18

Lemon RL, Doswell III CA (1979) Severe thunderstorm evolution and mesocyclone structure as related to tornadogenesis. Mon Wea Rev 107: 1184–1197

Liou YC, Luo I (2001) An investigation of the moving-frame single-Doppler wind retrieval technique using Taiwan area mesoscale experiment low-level data. J Appl Meteorol 40: 1900–1917

Liou YC, Gal-Chen T, Lilly DK (1991) Retrieval of winds, temperature and pressure from single-Doppler radar and a numerical model. Preprints, 25th Int. Conf. on Radar Meteor AMS 151–154

Nascimento E, Droegemeier KK (2002) Dynamic adjustment within an idealized numerically-simulated blow echo: implications for data assimilation. Preprints, Symposium on Observations, Data Assimilation, and Probabilistic Prediction, AMS, pp 13–17

Navon IM, Legler DM (1987) Conjugate-gradient methods for large-scale minimization in meteorology. Mon Wea Rev 115: 1479–1502

Qiu C-J, Xu Q (1992) A simple adjoint method of wind analysis for single-Doppler data. J Atmos Oceanic Technol 9: 588–598

Qiu C-J, Xu Q (1996) Least-square retrieval of microburst winds from single-Doppler radar data. Mon Wea Rev 124: 1132–1144

Rinehart RE (1979) Internal storm motions from a single non-Doppler weather radar. NCAR/TN-146 + STR, 262 pp

Sasaki Y (1970) Some basic formalisms in numerical variational analysis. Mon Wea Rev 98: 875–883

Shapiro A, Ellis S, Shaw J (1995) Single-Doppler radar retrievals with Phoenix II data: clear air and microburst wind retrievals in the planetary boundary layer. J Atmos Sci 52: 1265–1287

Shapiro A, Robinson P, Wurman J, Gao J (2003) Single-Doppler velocity retrieval with rapid-scan radar data. J Atmos Oceanic Technol 20: 1758–1775

Sun J, Crook NA (1997) Dynamical and microphysical retrieval from Doppler radar observations using a cloud model and its adjoint. Part I: Model development and simulated data experiments. J Atmos Sci 54: 1642–1661

Sun J, Crook NA (1998) Dynamical and microphysical retrieval from Doppler radar observations using a cloud model and its adjoint. Part II: Retrieval experiments of an observed Florida convective storm. J Atmos Sci 54: 1642–1661

Sun J, Flicker DW, Lilly DK (1991) Recovery of three-dimensional wind and temperature fields from simulated Doppler dadar data. J Atmos Sci 48: 876–890

Tuttle JD, Foote JB (1990) Determination of the boundary layer airflow from a single Doppler radar. J Atmos Oceanic Technol 7: 218–232

Weygandt S, Shapiro A, Droegemeier KK (1995) Adaptation of a single-Doppler retrieval for use on a deep-convection storm. Preprints, 27th Conf. on Radar Meteor, AMS, Vail, CO, pp 264–266

Weygandt S, Nutter P, Kalnay E, Park SK, Droegemeier KK (1999) The relative importance of different data fields in a numerically-simulated convective storm. Preprints, 8th Conf. on Mesoscale Processes, AMS, Boulder, CO, pp 310–315

Weygandt SS, Shapiro A, Droegemeier KK (2002) Retrieval of model initial fields from single-Doppler observations of a supercell thunderstorm. Part I: Single-Doppler velocity retrieval. Mon Wea Rev 130: 433–453

Xu Q, Qiu CJ, Yu J-X (1994a) Adjoint-method retrievals of low-altitude wind fields from single-Doppler reflectivity measured during Phoenix-II. J Atmos Oceanic Technol 11: 275–288

Xu Q, Qiu CJ (1994b) Simple adjoint methods for single-Doppler wind analysis with a strong constraint of mass conservation. J Atmos Oceanic Technol 11: 289–298

Xu Q, Qiu CJ (1995) Adjoint-method retrievals of low-altitude wind fields from single-Doppler reflectivity and radial-wind. J Atmos Oceanic Technol 12: 1111–1119

Xu Q, Gu H, Yang S (2001) Simple adjoint method for three-dimensional wind retrievals from single-Doppler radar. Quart J Roy Meteor Soc 127: 1053–1067

Xue M, Droegemeier KK, Wong V, Shapiro A, Brewster K (1995) ARPS Version 4.0 User's Guide, 380 pp [Available from http://www.caps.ou.edu/ARPS]

Xue M, Droegemeier KK, Wong V (2000) The Advanced Regional Prediction System (ARPS) – A multiscale nonhydrostatic atmospheric simulation and prediction tool. Part I: Model dynamics and verification. Meteorol Atmos Phys 75: 161–193

Zhang J, Gal-Chen T (1996) Single-Doppler wind retrieval in the moving frame of reference. J Atmos Sci 53: 2609–2623

Corresponding author's address: Jidong Gao, CAPS, University of Oklahoma, Sarkeys Energy Center, Suite 1110, 100 East Boyd, Norman, OK 73019, USA (E-mail: jdgao@ou.edu)